Proceedings of the ASME 2021 International Design Engineering Technical Conferences & Computers and Information in Engineering Conference
IDETC/CIE 2021
August 17-20, 2021, Online, Virtual,

IDETC/CIE2021-71918

GEOMETRY ENHANCED GENERATIVE ADVERSARIAL NETWORKS FOR RANDOM HETEROGENEOUS MATERIAL REPRESENTATION

Hongrui Chen
Department of Mechanical Engineering
Carnegie Mellon University
Pittsburgh,PA
Email: hongruic@andrew.cmu.edu

Xingchen Liu*
International Computer Science Institute
Berkeley, CA
Email: xingchen@icsi.berkeley.edu

ABSTRACT

The representation of material structure geometry is essential to the reconstruction, physical simulation, and the multiscale structure design with Random Heterogeneous Material (RHM). Traditional approaches to material structure representation often need to balance the trade-off between efficacy and accuracy. Recently, deep learning-based techniques have been adopted to reduce the computational time of RHM reconstruction. However, existing approaches generally lack guarantees over key RHM characteristics, including Minkowski functionals and correlation functions.

We propose a novel approach to geometrically enhancing the deep learning-based RHM representation by introducing Minkowski functionals, a set of topological and geometrical characteristics of material structure, into the training of conditional Generative Adversarial Networks (cGAN). This hybrid approach combines the feature learning capability of deep learning with the well-established material structure characteristics, greatly improving the accuracy of the RHM representation while maintaining its efficiency. The effectiveness of the proposed hybrid approach is validated through the reconstruction of a wide range of natural and manmade materials, including Voronoi foam structures, femur, and sandstone. Through computational experiments, we demonstrate that geometrically enhancing the training of cGAN for RHM representation not only significantly decreases the representation error in Minkowski functionals between input sample materials and reconstructed results, but also improves the performance of other material structure characteristics, such as two-point correlation functions.

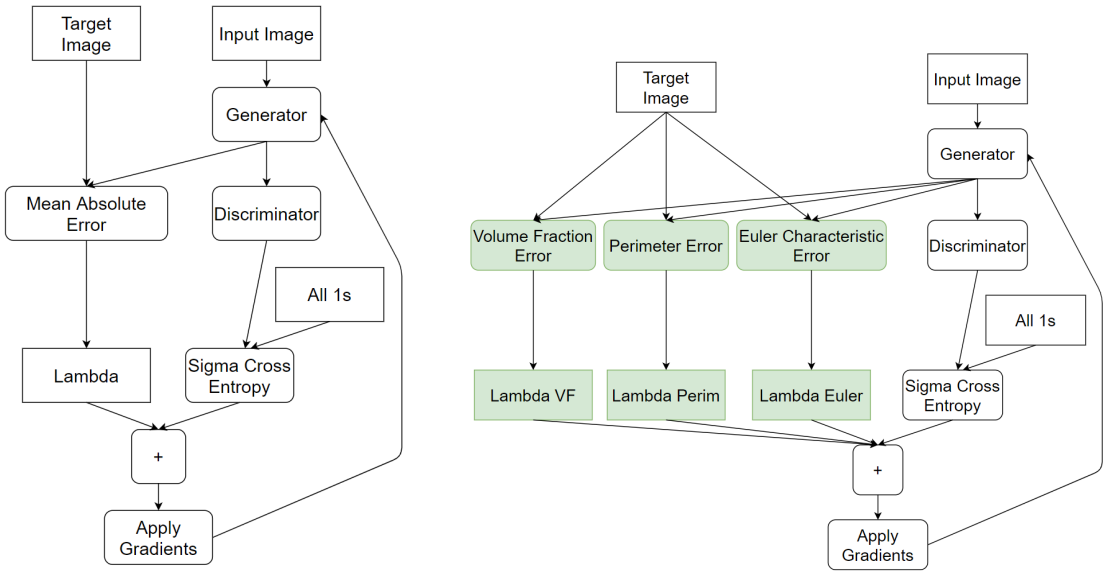
Keywords: Material Structure Representation, Multiscale Structure, Generative Adversarial Networks, Minkowski Functional, Correlation Functions

1 INTRODUCTION

Material structures represent a crucial part in characterizing the overall mechanical performance of components across the scales. Nature itself exploits the advantages of manipulating material structure. From the porous structure of tree bark that carries nutrients from roots to leaves to the delicate structures within bones that distribute the load from each joint. Through material structures, nature achieved spectacular results that are difficult for homogeneous materials to rival. To capture the capabilities of material structure design, various methods of recreation and generation had been developed. Early approaches rely on material characteristics such as low order correlation functions. However, they do not preserve geometry details as two very different random heterogeneous materials (RHM) may have very similar low order correlation functions [1]. The texture synthesis-based approach is the first approach to accurately preserve geometric details in RHM reconstructions [2]. Numerous studies also enhanced texture synthesis by using it as a design tool by adapting the structures with prescribed physical properties [3,4]. Texture synthesis demonstrated promising results in designing material structures. However, as most texture synthesis relies on generat-

*Address all correspondence to this author.

Copyright © 2021 by ASME



(a) cGAN loss

(b) cGAN + MFGAN loss

FIGURE 1: Comparing the loss function for cGAN and MFGAN. MFGAN incorporates the differences in Minkowski functionals between the generated structures and ground truth structures in addition to the GAN loss.

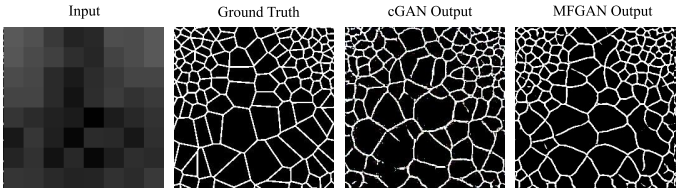


FIGURE 2: Sample Voronoi cell synthesis results via cGAN and MFGAN. We observed that there are disconnected edges in the cGAN outputs which motivates the addition of Minkowski functionals into GAN.

ing single-pixel or very small patches at once, as the complexity of the baseline texture or the size of the final target increases, the generation time increases dramatically.

Over the last few years, deep learning techniques, such as the Convolutional Neural Network (CNN) [5], drastically improved the state-of-the-art in speech recognition, visual object recognition, and object detection, to list a few. In contrast to the traditionally fully connected networks, CNN takes advantage of the hierarchical pattern in data and assembles more complex patterns using smaller and simpler patterns. A typical CNN, e.g. VGG-16 [6], has two parts, convolutional layers learn the features in the training dataset while fully-connected layers perform the traditional classification tasks. Recently, the feature learning capability of CNN has been used in the reconstruction of RHM [6], where an iterative process gradually reduces the difference between the generated and exemplar RHM in the feature space. The iterative process of RHM reconstruction is computationally expensive as the reconstructed RHMs need to be repeatedly passed through the CNN to evaluate their features. So, fundamentally, this is similar to the iterative approach, but the characterization is done through either feature learning or transfer learning.

On the other hand, recent progress in machine learning-enabled an exponential increase in research into computer vision and image processing. Among such progress is Generative Adversarial Networks (GAN) [7]. First proposed by Goodfellow, GAN consists of two competing neural networks namely the generator and the discriminator. The purpose of the generator is to generate images based on a given input, while the discriminator judges the quality of the generated images. During the training of GAN, the two neural networks evolve together as the generator tries to generate images that the discriminator cannot discern as "real" or "fake" and the discriminator tries to catch the generator's "fake" image. With the invention of GAN, much research that follows improved the capability of GAN. One such improvement is Pix2Pix [8]. In contrast to the original GAN that relies on random noise or a vector as inputs for the generator, Pix2Pix's generator takes in a two-dimensional image. Through the use of neural networks, GAN enables a variety of tasks that originally take a longer time to perform, such as transforming satellite imagery into maps or hand sketches into photos.

Indeed, representing material structure is one of the tasks that can be augmented by GAN. GAN enables the faster synthesis of

Copyright © 2021 by ASME

material structures compared to texture synthesis methods. Previous research has demonstrated that latent variables can serve as design variables to the generator [9]. However, higher dimensional latent variables such as images not only could represent higher dimensions of design variables such as a physical or material property field but also enables complex multiscale design with RHM structures.

Characterization of material structures allows comparison and quantitative analysis of various RHM representations. One such common characteristic of the material structure is the Minkowski functionals, which include Euler characteristics, perimeter, volume in 2D, and the 3D perimeter is replaced by surface area and mean breadth as an additional term. Minkowski functionals encompass many criteria for analyzing material structure. Previous research used the Euler characteristic, one of the Minkowski functionals, to compare the generated structure from GAN [10]. While useful for characterization, it would be beneficial if Minkowski functionals can aid the training and feature learning in GAN. The main contribution of this paper is: to improve the topological and geometrical characteristics of the generated structure by incorporating Minkowski functionals into the GAN architecture as a loss function of the generator. During the training phase, the proposed network architecture minimizes the mismatch of Minkowski functionals between the training sample and generated structures. A fully differentiable algorithm for Minkowski functionals computation is implemented to enable the full capabilities of backpropagation in the training of networks. We call the proposed network Minkowski Functional Generative Adversarial Network (MFGAN).

The rest of this paper will be organized as follows. In Section 2, we review the current progress in material structure synthesis. Then we introduce the core concept of GAN and followed by a discussion of Minkowski functionals. In Section 3, we present the detailed implementation of our proposed method. Specifically, a fully differentiable algorithm for Minkowski functionals computation for backpropagation. We then showcase the result of our proposed method in Section 4. We demonstrate MFGAN creates not only visually similar but also with the help of adding Minkowski functionals more geometrically accurate structure synthesis. Finally, we conclude with discussions in Section 5.

2 RELATED WORK

2.1 RHM Representation and Reconstruction

The simplest way to characterize RHM is through volume fraction. Volume fraction refers to the ratio between the solid and total volume of a given material structure. While commonly used, volume fraction characterization lacks information about the geometry and topology of the material structure. In addition, the material structure of a heterogeneous material may be parameterized as a typical "unit cell" located at a "location" in space, which is usually referred to as a grain - germ model. Both the shape and location of the unit cell are governed by some physically justified stochastic process. The advantage of this approach includes the ability to explicitly control, vary, parameterize, and synthesize the material structure procedurally. Unfortunately, only limited classes of materials with simple unit cell geometry and distributions can be accurately modeled since the modeling process requires complete understanding and parameterization of the generative process underlying material – a challenging task even for most common materials such as sandstone.

The limited heterogeneous materials that the grain - germ model can model lead to the belief that heterogeneous materials are too complex to model other ways but statistically. In statistics-based models, heterogeneous materials are abstracted by their low-order statistics, such as volume fraction and two-point correlation functions [11, 12]. A large-scale stochastic optimization problem is often solved by iteratively matching the statistics. One advantage of the statistics-based approach is its applicability to a broad range of random heterogeneous materials because it does not depend on the stochastic process by which a material structure is formed [13]. However, once the material structure is abstracted by its low-order statistics, important geometric and topological details of the material are usually lost. As a result, different material structures with similar two-point correlation functions may lead to similar models [3]. The stationarity of the material is often assumed since correlation functions are usually measured through the entire material sample and are not equipped to parameterize information across different scales.

The sample-based approach is successful in the reconstruction of random heterogeneous materials and the synthesis of two-scale structures with random heterogeneous materials on the fine-scale [14, 15, 16]. Conceptually, the RHM is modeled via Markov random fields, representing the material structure as a collection of neighborhoods. Initially, the approach is used to reconstruct stationary RHM, where multiple statistically equivalent samples of various sizes are generated to support the further evaluation of the material [2]. The method is shown to preserve the joint probabilities and other statistical measures, as well as the mechanical property of the sample material structure. Later, the sample-based approach is extended to design two-scale structures with RHM on the fine-scale. Previous research by Liu and Shapiro has demonstrated several successful applications in designing novel multiscale structures with RHM, including the design of functionally graded material structures with controlled spatially varying effective material properties on the coarse-scale [3, 2] and the design of two-scale structures with anisotropic RHM on the fine-scale and controlled variation of orientation-dependent effective material properties on the coarse-scale [3]. Even though successful implementations have been demonstrated in both two and three dimensions, the sample-based approach still requires significant computational resources to process three-dimensional material structure data.

Copyright © 2021 by ASME

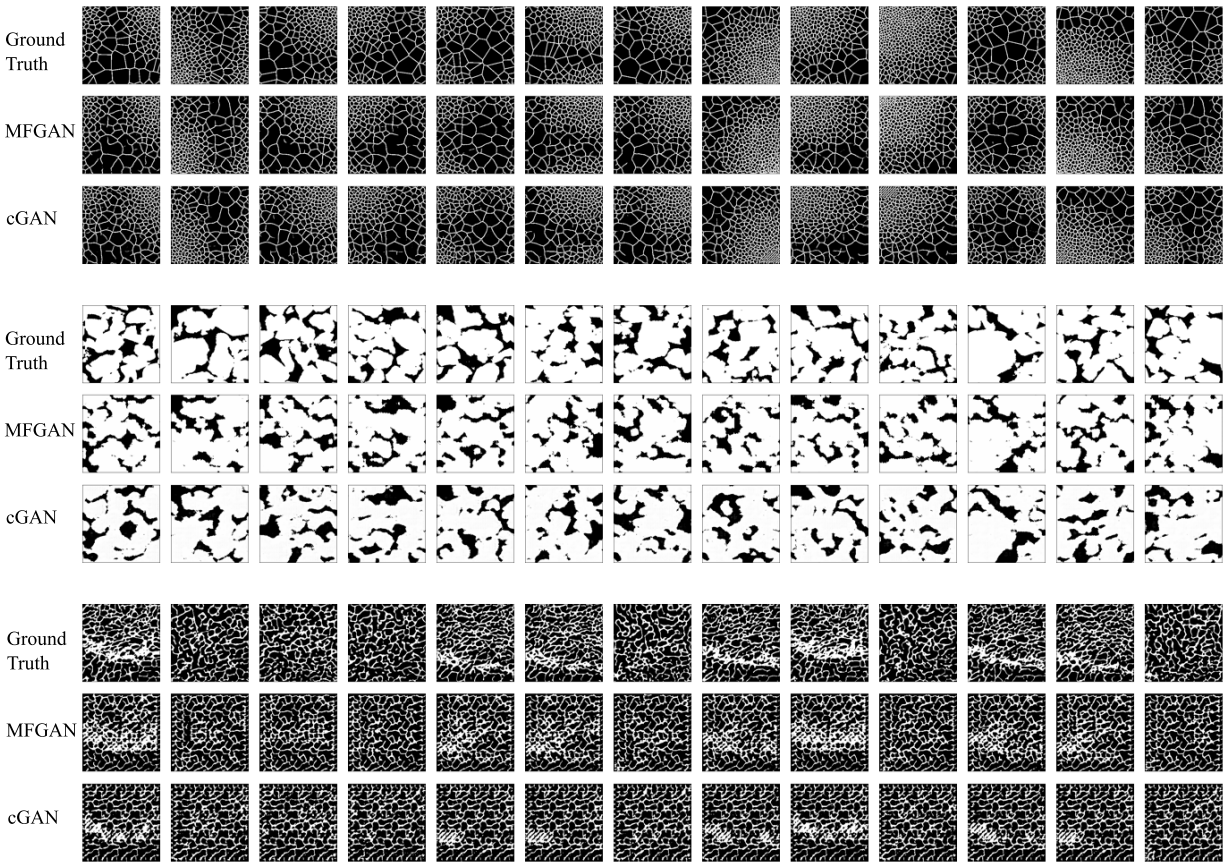


FIGURE 3: Comparison of outputs from MFGAN and cGAN from the Voronoi, sandstone, and femur dataset

2.2 Deep Learning in RHM representation

Deep learning techniques show great potential to increase the efficiency of the sample-based design algorithm. The most relevant results on deep learning to the proposed investigation are in the domain of computer vision and image recognition. The first breakthrough of the Convolutional Neural Network (CNN) is almost halving the error rate for object recognition [17]. The work precipitated the rapid adoption of deep learning by the computer vision community. One of the challenges in the modeling of RHM is the lack of proper representation. CNN learns complex representations through the composition of many simple but non-linear transformations with minimal engineering by hand. Using the feature learning capability, Bostanabad casts the RHM reconstruction task as an optimization problem where a random 3D image is iteratively refined to match its microstructural features to those of the exemplar [18]. VGG19, a pre-trained deep convolutional neural network, is used to obtain the microstructural features and construct the objective function. In addition, Cang et al. developed a feature learning mechanism based on a convolutional deep belief network (CDBN) to automate a two-way conversion between material structures and their lower-dimensional feature representations, achieving a 1000-fold dimension reduction from the material structure space [19]. Currently, this method can only be used for 2D RHM reconstruction, and it cannot guarantee the accuracy, because the key parameters such as threshold are determined empirically. Using CNN to extract the feature for RHM reconstruction is not fundamentally different from the large-scale stochastic optimization approach that matches the statistics of RHM. Granted, a much larger set of features is used for shape matching; however, the many geometric and topological characteristics that directly link to the physical performance of the material are no longer preserved.

The applications of deep learning remained mostly diagnostic until the invention of GAN. First proposed by Goodfellow, GAN can accomplish almost the reverse of ordinary neural networks by generating samples similar to the training dataset [7]. Ever since the introduction of GAN, there have been many variations to its architecture to accomplish tasks related to image generation. GAN can be used to upscale textures from old video games [20]. Other applications of GAN involve transforming hand-drawn im-

Copyright © 2021 by ASME

TABLE 1: Hyperparameters for both cGAN and MFGAN training.

Parameter	Learning Rate	Batch Size	Epoch
Value	1e-4	2	40

ages to photos, satellite images to maps, and changing the style of photos [21]. With almost endless possibilities, GAN had been also extended to material structure synthesis. Related research includes using GAN to learn the mapping between latent variables and material structures [22]. The use of latent variables could be less intuitive when used as a design tool for material structure synthesis. An additional Convolutional Neural Network (CNN) can be attached to the GAN such that the CNN can evaluate the compliance tensor of the generated material structure in which ultimately training the GAN to generate material structures with similar compliance tensor as given samples [23]. StyleGAN has also been adapted to material structure synthesis [10]. Fokina et. al. compared the generation result of GAN from real material structures and found out that GAN can generate material structures with similar Minkowski functionals [10]. However, in our experiment, we observe that such property no longer holds for more complex material structures, such as Voronoi foam.

2.3 Material structure Characterization

Minkowski functionals are a set of topological and geometrical descriptors of material structures. It encompassed d+1 functionals in d-dimensional space. For a 2D material structure, its Minkowski functionals include area, perimeter, and Euler characteristics. For 3D material structure, there are four Minkowski functionals, including volume, surface area, mean width, and Euler characteristics. Minkowski functionals have been applied as a method of characterizing and accessing the material structure performance of generated or reconstructed materials. For example, Minkowski functions have been applied to evaluate the material structure reconstructed by the texture synthesis-based approach [2]. As mentioned in the previous section, recent research also used Minkowski functionals to characterize and compare the result of GAN-generated material structures [10]. In the current work, we introduce Minkowski functionals directly into the deep learning network training process.

Correlation functions. An n-point correlation function can be defined as the probability that all vertices of a randomly tossed n-vertex polyhedron fall into the same phase of a material structure [13]. Two-point and three-point correlation functions are known to correlate closely with elastic stiffness of the material [13], while strain localization and damage evolution are sensitive to higher-order correlation [24]. Generally speaking, higher-order correlation functions yield more information about the material, and the ability of lower-order correlation functions to predict many material properties, e.g., those that depend on connectivity, is still undetermined [25]. Two-point correlation functions are used in the current paper to characterize and compare the quality of RHM representation with and without Minkowski functionals.

3 GEOMETRY ENHANCED GAN

3.1 RHM Representation with GAN

We construct our network based on the architecture of Pix2Pix [8]. There are several key advantages to this approach compared to other variations of GANs. First, the conditional input to the generator is of the same physical size and dimension as the output, allowing various material characterizations and properties, such as Minkowski functionals and effective stiffness, to be directly used as the input to control the RHM synthesis process. Compared to other GAN architectures using one-dimensional latent vectors, an intuitive and straightforward correspondence between the input and outputs may be established. This not only facilitates the direct visual inspection of the generated results but also enables more complex relationships between input and the target image to be learned without any additional pre-and/or post-processing. Another key advantage of the Pix2Pix architecture is the capability of learning from a small number of training samples compared to the regular/vanilla GAN. The use of a patch-based discriminator (PatchGAN) contributes to the improved learning capability over a small number of samples. This is important for material structure modeling as the training dataset is often limited compared to computer vision applications. In the current paper, we experimented with 100 to 200 training samples. Specifically, the training sample is two 256x256 resolution images concatenated together. The image on the left is the sample material structure which will be referred to as "target". The field image is placed on the right. The field image can be generated in multiple ways. All of the experiment results in this paper used a downsampled density field of the original material structure. In the current work, we focused on the 2D reconstruction of material structures as a proof of concept. However, both GAN and Minkowski functionals calculation can be extended into the 3D material structure and we developed our model with future 3D expansion in mind. The generator consists of convolution layers stacked together followed by deconvolution layers. In addition, the convolution and deconvolution layers are connected with skip connectors. The discriminator consists of convolution layers to downsample the generated image from the original resolution to a lower resolution. For a more in-depth discussion about network architecture, please refer to this paper [8].

We used the following hyperparameters listed in Table 1 during training. The GAN is implemented in TensorFlow 2.4.1. The optimizer is the built-in Adam optimizer. The training time of the network takes around 10-20 minutes depending on the sample dataset size. During training, we recorded the loss values of the network and after training was finished, the network was saved for further evaluation.

Copyright © 2021 by ASME

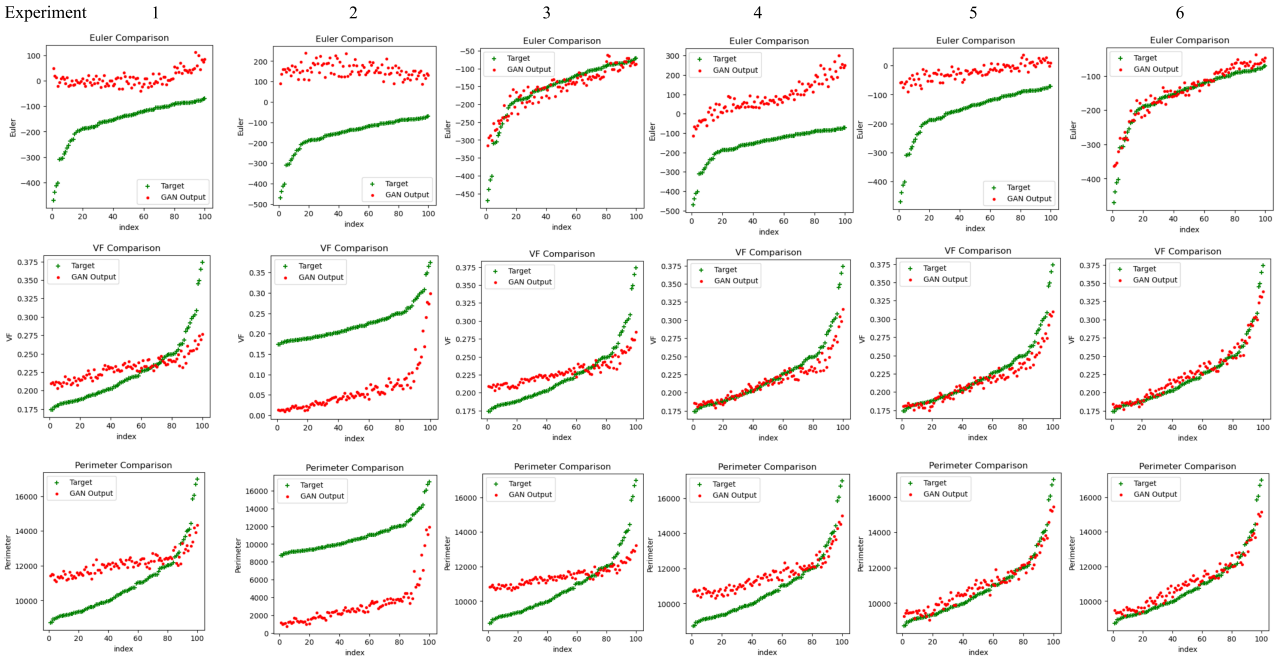


FIGURE 4: Visualization on the difference in Minkowski functionals (MFs) between the training and generated material structures. The plot shows results from 6 experiments with and without using MFs in the network training and their individual effects. The corresponding hyperparameters are listed in Table 2. To help visualization, we sorted the testing dataset's Minkowski functionals values in ascending order. The closer red dots to green dots distribution, the more accurate GAN's reconstruction is.

One popular approach to creating artificial functionally graded materials is to use Voronoi cells since the material distribution can be easily and straightforwardly controlled [26]. A functionally graded Voronoi foam structure is created by controlling the spacing between Voronoi seeds.

Although straightforward by definition, creating Voronoi cells can be time-consuming. The MATLAB program we use to generate the training set takes around 2 seconds for one Voronoi structure. Samples of these Vornoi structures are shown in Figure 2 as ground truth for the neural network training. We also generate an 8 by 8 density field by downsampling the ground truth material structure as input to the generator. This density field allows us to control the material property distribution on the coarse scale for two-scale structures design [27]. After training, the neural network learned the gradation of the input density field. However, shown in Figure 2, many of the edges of the Voronoi cells are disconnected in the cGAN generated material structures . Calculating and comparing the Euler characteristic number confirms our observations. This preliminary investigation shows large errors in Minkowski functionals and correlation functions compared to the training sample. The result for cGAN is summarized in Table 2 as experiment 1. In the original Pix2Pix implementation [8], L1 loss between training dataset and GAN output is also used, we observed the addition of L1 loss performs poorly in microstructure reconstruction (see Table 1 experiment 2). In the next section, we experiment with a hybrid approach by incorporating Minkowski functionals into the GAN training process to resolve this issue to improve the quality of synthesized structure.

3.2 Minkowski Functionals for Geometry Enhanced GAN

We incorporate the Minkowski functionals into the GAN training by adding the difference in Minkowski functionals between the generated material structure and ground truth into the loss function in addition to the loss term from the discriminator. The procedure of computing Minkowski functionals over the image is well known and an open-source library is available in MATLAB for pixelated structures [28]. However, we could not use this library directly as it relies on logic values whereas continuous values are preferred to take advantage of automatic differentiation features for neural networks. Instead, we extend the Minkowski functionals calculation into continuous space. We provide a detailed description of Minkowski functional calculations in the Appendix.

We apply normalization to the Minkowski functionals and

Copyright © 2021 by ASME

TABLE 2: Comparison between different configurations of hyperparameters and Minkowski functionals L1 loss computed. With full incorporation of Minkowski functionals as loss, we observed improvements in all L1 loss values compared to cGAN.

	Training Hyperparameters					Result		
Experiment #	GAN Loss	L1 Loss	λ_{Euler}	λ_{Perim}	λ_{VF}	Euler L1 Loss	VF L1 Loss	Perim L1 Loss
1	1.0	0.0	0.0	0.0	0.0	165.73	0.02415	1572.76
2	1.0	100.0	0.0	0.0	0.0	311.298	0.16224	7783.64
3	1.0	0.0	0.05	0.0	0.0	21.79	0.02167	1194.48
4	1.0	0.0	0.0	0.0	1000.0	240.24	0.0109	1006.99
5	1.0	0.0	0.0	0.05	0.0	135.63	0.0104	399.87
6	1.0	0.0	0.05	0.05	1000.0	17.44	0.0007	446.02

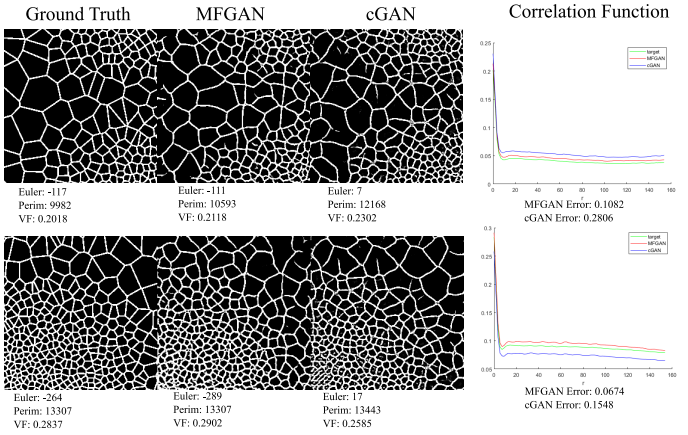


FIGURE 5: Correlation function comparison of one sample between target (red), experiment #6 (green), experiment #1 (blue). With the addition of Minkowski functionals, the relative error is significantly lower

compute the L1 loss between output and target material structures. Finally, a weight is applied to each of the Minkowski functional losses such that we can fine-tune the network. Figure 4 and Table 2 provides a comparison between the original cGAN vs our implementation. One potential concern about directly calculating Minkowski functionals on the normalized output is that the neural network output is continuous within a range whereas the previous implementation of Minkowski functionals expects a logical integer value [28]. We could use a logistic function to map the output distribution more closely to -1 and 1. However, we observed that when the training converges, the output of the neural network already distributes closely between -1 and 1.

During training, the generator can take into account the difference in Minkowski functionals between generated material structures and their corresponding ground truth. Since the Minkowski functionals are a part of the loss function, the network will attempt to decrease the total loss thus creating material structures that resemble more its training target. In the case of minimizing the difference between Euler numbers, this will push the neural network to generate structures with better connectivity thus reducing the disconnected edges.

In our implementation, we set λ values as coefficients multiplied by each of the Minkowski functionals. In addition, to prevent these Minkowski functionals from causing the neural network to be stuck in a local minimum, we begin with a very small lambda and gradually increase it during training. To determine the effect of each Minkowski functionals, we run tests with different combinations of λ. The results are summarized in Table 2. We note that errors in perimeter could decrease even with only Euler loss being added into the loss functions. This demonstrates that the effect of the Euler number not only decreased the corresponding error but also improved the overall accuracy of the deep learning-based representation. We also compare the two-point correlation function of the generated versus the ground truth material structure. The average relative errors for all 100 test samples in the correlation function are 0.0779 for Experiment #6 and 0.1332, a 42% reduction in error. This is achieved without the direct inclusion of correlation functions in the network training process, demonstrating that Minkowski functionals indeed improve the quality of RHM representation.

4 EXPERIMENT RESULTS

We trained the GAN on a desktop computer with Core i7-6700@3.2 GHz, 32GB RAM, and NVIDIA GeForce GTX 1080Ti on Windows 10 ver. 20H2. The training datasets were generated from both Python and MATLAB with externally obtained 3D material structure data. The images used in the dataset are 256 by 256 resolution.

After training is finished, we save the generator and discard the discriminator since the generator is the network that reconstructs the material structure. We observe that the result from

Copyright © 2021 by ASME

TABLE 3: Loss comparison on the sandstone dataset

Sandstone	Euler L1 loss	Perimeter L1 loss	VF L1 loss	Relative error in correlation function
MFGAN	8.84	257.87	0.024	0.0516
cGAN	142.19	548.81	0.027	0.0597

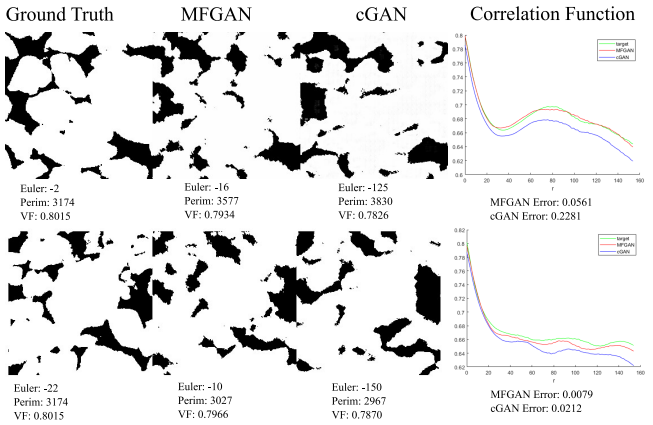


FIGURE 6: Comparison of MFGAN and cGAN on the sandstone dataset. MFGAN improved the Euler characteristics greatly with marginal improvements in VF and perimeter.

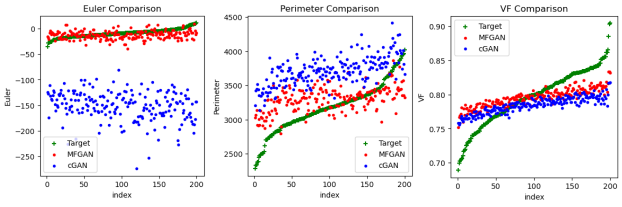


FIGURE 7: Comparison of Minkowski functionals for MFGAN and cGAN on the sandstone dataset.

the generated material structure indeed resembles those of the target images. The edge lines are sharp and crisp with very low noise. In addition, we can also design the density field and use the trained model to generate the corresponding material structures. The average speed of generating one image is 30 ms. Furthermore, TensorFlow neural network models also allow us to pass multiple input images in a batch into the model. Depending on the performance of the CPU and GPU, the speed can be faster per image when using a batch.

4.1 Sandstone

Sandstone is a rock that is composed of small silicate grains. We obtained the dataset from Imperial College London Department of Earth Science and Engineering's Micro-CT Images. The raw data for the sandstone is a binary length 1000 voxels cube. We slice and then crop the cube to obtain material structures with resolution 256 by 256. We generate an 8 by 8 density field as the input of the cGAN.

TABLE 4: Loss comparison on the femur dataset

Femur	Euler L1 loss	Perimeter L1 loss	VF L1 loss	Relative error in correlation function
MFGAN	12.77	542.59	0.011	0.0582
cGAN	101.03	823.47	0.025	0.1561

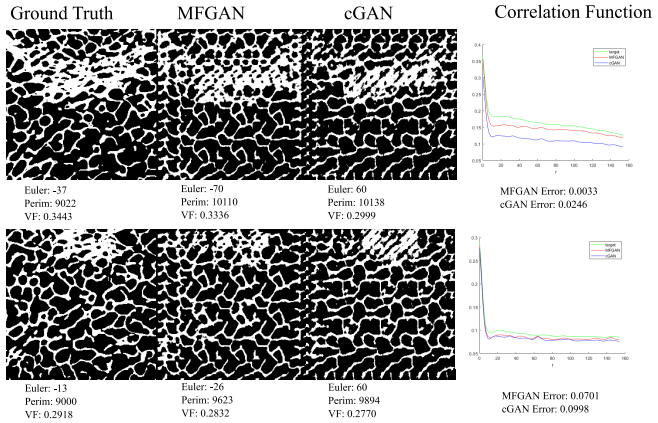


FIGURE 8: Comparison of MFGAN and cGAN on the femur dataset.

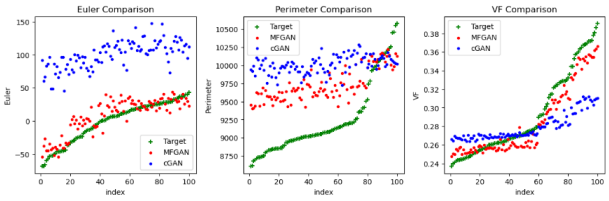


FIGURE 9: Comparison of Minkowski functionals for MFGAN and cGAN on the femur dataset.

We compared the results of MFGAN and cGAN through material structure characteristics. Firstly, MFGAN reduced L1 loss in all three Minkowski functionals. The most significant reduction is in Euler numbers. Both perimeter and VF also saw a decrease in loss. For correlation function, most likely due to the stationary nature of sandstone, cGAN already has achieved a low relative error in the correlation function. Nevertheless, we still observed a reduction in relative error in correlation function.

Copyright © 2021 by ASME

4.2 Femur

Sandstones can be considered as a type of stationary material. The term stationary refers to the fact that when we change location in the material structure space, the statistics describing the material don't change. On the other hand, the cross-section of the femur showed that it is a non-stationary material. Specifically, the femur is a functionally graded material where the gradation serves a biological function. In the case of the femur, the gradation helps the bone to prevent bending and distribute the load evenly while maintaining a lower mass compared to pure solid structures. We used similar procedures to generate the training and testing dataset. The results are shown in Figure 8.

When comparing the result from MFGAN and cGAN, we observed similar improvements compared to the sandstone dataset on Minkowski functionals. In terms of the correlation function, the improvement is on par with the Voronoi cells dataset. MFGAN reduced 63% of the relative error in correlation function. Visually, the results from MFGAN have less noise compared to the cGAN.

5 CONCLUSION

The present work demonstrated the versatility of MFGAN's application in material structure synthesis through four types of material structures. In all four cases, MFGAN learned the material distribution and synthesized compelling material structures. To further increase the synthesis accuracy, we exploited the power of neural networks and added Minkowski functionals into the architecture. With this hybrid approach, we not only decreased the error in Minkowski functionals of synthesized material structures but also observed the additional benefit of decreasing the relative error in the correlation function.

Compared to less efficient traditional approaches, MFGAN can be used in generating material structures for multiscale topology and material optimizations . We are currently working on further exploring the capabilities of MFGAN's application in material structure synthesis. Currently, the Minkowski functionals are evaluated for the entire structure. This could lead to local differences in Minkowski functionals being averaged out. One way to alleviate this issue is to calculate Minkowski functionals patch by patch. Also, Minkowski functionals and correlation functions are based on the geometry of the material structure. Although they are important characteristics, one can also evaluate material structure from their mechanical characteristics. Stiffness tensors can also be evaluated even incorporated into the network architecture. Finally, material structures of larger resolution can be generated by connecting patches of smaller material structures together. The current MFGAN can be modified and adapted to synthesize large-scale material structures while maintaining a low computational cost.

ACKNOWLEDGEMENTS

This research was partially supported by the Defense Advanced Research Projects Agency. The responsibility for errors and omissions lies solely with the author.

REFERENCES

[1] Corson, P. B., 1974. "Correlation functions for predicting properties of heterogeneous materials. I. Experimental measurement of spatial correlation functions in multiphase solids". *Journal of Applied Physics,* ***45***(7), pp. 3159–3164.

[2] Liu, X., and Shapiro, V., 2015. "Random heterogeneous materials via texture synthesis". *Computational Materials Science,* ***99***, mar, pp. 177–189.

[3] Liu, X., and Shapiro, V., 2017. "Sample-based synthesis of two-scale structures with anisotropy". *CAD Computer Aided Design,* ***90***, sep, pp. 199–209.

[4] Liu, X., and Shapiro, V., 2017. "Sample-Based Synthesis of Functionally Graded Material Structures". *Journal of Computing and Information Science in Engineering,* ***17***(3), p. 31012.

[5] Russakovsky, O., Deng, J., Su, H., Krause, J., Satheesh, S., Ma, S., Huang, Z., Karpathy, A., Khosla, A., Bernstein, M., Berg, A. C., and Fei-Fei, L., 2015. "ImageNet Large Scale Visual Recognition Challenge". *International Journal of Computer Vision,* ***115***(3), pp. 211–252.

[6] Simonyan, K., and Zisserman, A., 2014. "Very deep convolutional networks for large-scale image recognition". *arXiv preprint arXiv:1409.1556*.

[7] Goodfellow, I. J., Pouget-Abadie, J., Mirza, M., Xu, B., Warde-Farley, D., Ozair, S., Courville, A., and Bengio, Y., 2014. "Generative Adversarial Networks". *Advances in Neural Information Processing Systems 27*.

[8] Isola, P., Zhu, J. Y., Zhou, T., and Efros, A. A., 2017. "Image-to-image translation with conditional adversarial networks". In Proceedings - 30th IEEE Conference on Computer Vision and Pattern Recognition, CVPR 2017, Vol. 2017-Janua, pp. 5967–5976.

[9] Li, X., Yang, Z., Brinson, L. C., Choudhary, A., Agrawal, A., and Chen, W., 2018. "A Deep Adversarial Learning Methodology for Designing Microstructural Material Systems".

[10] Fokina, D., Muravleva, E., Ovchinnikov, G., and Oseledets, I., 2020. "Microstructure synthesis using style-based generative adversarial networks". *Physical Review E,* ***101***, p. 43308.

[11] Yeong, C., and Torquato, S., 1998. "Reconstructing random media". *Physical Review E,* ***58***(1), jul, pp. 224–233.

[12] Xu, H., Li, Y., Brinson, C., and Chen, W., 2014. "A Descriptor-Based Design Methodology for Developing Heterogeneous Microstructural Materials System". *Journal of Mechanical Design,* ***136***(5), mar, p. 51007.

Copyright © 2021 by ASME

[13] Torquato, S., 2002. "Statistical Description of Microstructures". *Annual Review of Materials Research,* ***32***(1), aug, pp. 77–111.
[14] Bostanabad, R., Bui, A. T., Xie, W., Apley, D. W., and Chen, W., 2016. "Stochastic microstructure characterization and reconstruction via supervised learning". *Acta Materialia,* ***103***, pp. 89–102.
[15] Cang, R., and Ren, M. Y., 2016. "Deep Network-Based Feature Extraction and Reconstruction of Complex Material Microstructures". In Volume 2B: 42nd Design Automation Conference, no. 50114, ASME, p. V02BT03A008.
[16] Acar, P., and Sundararaghavan, V., 2016. "A Markov random field approach for modeling spatio-temporal evolution of microstructures". *Modelling and Simulation in Materials Science and Engineering,* ***24***(7), oct, p. 75005.
[17] Krizhevsky, A., Sutskever, I., and Hinton, G. E., 2012. "Imagenet classification with deep convolutional neural networks". In Advances in neural information processing systems, pp. 1097–1105.
[18] Bostanabad, R., 2020. "Reconstruction of 3D Microstructures from 2D Images via Transfer Learning". *CAD Computer Aided Design,* ***128***, nov, p. 102906.
[19] Cang, R., Xu, Y., Chen, S., Liu, Y., Jiao, Y., and Ren, M. Y., 2017. "Microstructure Representation and Reconstruction of Heterogeneous Materials Via Deep Belief Network for Computational Material Design". *Journal of Mechanical Design, Transactions of the ASME,* ***139***(7), jul.
[20] Ledig, C., Theis, L., Huszar, F., Caballero, J., Cunningham, A., Acosta, A., Aitken, A., Tejani, A., Totz, J., Wang, Z., and Shi, W., 2016. "Photo-Realistic Single Image Super-Resolution Using a Generative Adversarial Network". *Proceedings - 30th IEEE Conference on Computer Vision and Pattern Recognition, CVPR 2017,* ***2017-January***, sep, pp. 105–114.
[21] Efros, A. A., and Hertzmann, A., 2020. "When the adversary is your friend: technical perspective". *Communications of the ACM,* ***63***(11), p. 138.
[22] Yang, Z., Yabansu, Y. C., Al-Bahrani, R., keng Liao, W., Choudhary, A. N., Kalidindi, S. R., and Agrawal, A., 2018. "Deep learning approaches for mining structure-property linkages in high contrast composites from simulation datasets". *Computational Materials Science,* ***151***, aug, pp. 278–287.
[23] Tan, R. K., Zhang, N. L., and Ye, W. "A deep learning-based method for the design of microstructural materials".
[24] McDowell, D. L., Ghosh, S., and Kalidindi, S. R., 2011. "Representation and computational structure-property relations of random media". *Jom,* ***63***(3), mar, pp. 45–51.
[25] Fullwood, D. T., Niezgoda, S. R., Adams, B. L., and Kalidindi, S. R., 2010. "Microstructure sensitive design for performance optimization". *Progress in Materials Science,* ***55***(6), aug, pp. 477–562.
[26] Martínez, J., Dumas, J., and Lefebvre, S., 2016. "Procedural voronoi foams for additive manufacturing". *ACM Transactions on Graphics,* ***35***(4), pp. 1–12.
[27] Liu, X., and Shapiro, V., 2018. "Multiscale shape–material modeling by composition". *Computer-Aided Design,* ***102***, pp. 194–203.
[28] Lehmann, G., Legland, D., and Génie, U. M. R., 2012. "Efficient N-Dimensional surface estimation using Crofton formula and run-length encoding". pp. 1–11.

Appendix

Equations of each Minkowski function are provided below. For all of the equations below, x represents the pixelated microstructure image with a resolution of n by m.

$$VF = \frac{1}{nm}\sum_{i=1}^{n}\sum_{j=1}^{m} x \tag{1}$$

The first Minkowski functional is the volume(3D)/area(2D). Volume fraction can be calculated as the mean value of a given material structure sample and is more commonly used in material structure-related research [2].

$$\begin{aligned} P = \frac{\pi}{4}[(\frac{2\sqrt{2}+2}{\sqrt{2}}\sum_{i=1}^{n}\sum_{j=1}^{m} x) \\ -(\sum_{i=1}^{n-1}\sum_{j=1}^{m} x_{1:n-1,1:m}x_{2:n,1:m} + \sum_{i=1}^{n}\sum_{j=1}^{m-1} x_{1:n,1:m-1}x_{1:n,2:m} \\ + \frac{1}{\sqrt{2}}\sum_{i=1}^{n-1}\sum_{j=1}^{m-1} x_{1:n-1,1:m-1}x_{2:n,2:m} + \frac{1}{\sqrt{2}}\sum_{i=1}^{n-1}\sum_{j=1}^{m-1} x_{1:n-1,2:m}x_{2:n,1:m-1})] \end{aligned} \tag{2}$$

The second Minkowski functional is P/2 where P is the perimeter. We implemented a perimeter approximation using simple matrix operation by assuming 4-neighbors connectivity. The third Minkowski functional is the Euler characteristic. Euler characteristic is also referred to as Euler number. Euler number is very useful in providing a characterization of the geometry of the material structure. The Euler number can be calculated as follows:

$$\begin{aligned} \chi = \sum_{i=1}^{n}\sum_{j=1}^{m} x - \sum_{i=1}^{n-1}\sum_{j=1}^{m} x_{1:n-1,1:m}x_{2:n,1:m} - \sum_{i=1}^{n}\sum_{j=1}^{m-1} x_{1:n,1:m-1}x_{1:n,2:m} \\ + \sum_{i=1}^{n-1}\sum_{j=1}^{m-1} x_{1:n-1,1:m-1}x_{2:n,1:m-1}x_{2:n-1,2:m}x_{1:n-1,2:m} \end{aligned} \tag{3}$$

Copyright © 2021 by ASME